Slow Scintillation Component and Radiation-Induced Readout Noise in Undoped CsI Crystals

Fan Yang, *Member, IEEE*, Liyuan Zhang, *Member, IEEE*, Chen Hu, *Member, IEEE*, and Ren-Yuan Zhu, *Senior Member, IEEE*

***Abstract*— Because of its fast scintillation and low cost, undoped CsI crystal has been used to construct crystal calorimeters for high-energy physics experiments. Undoped CsI crystal samples from three vendors were investigated at the Caltech Crystal Laboratory. In addition to the 30-ns fast scintillation peaked at 310 nm, a slow scintillation component peaked at 450 nm was found with a decay time of a few microseconds. The intensity of the slow component may be varied from the seed to the tail end, so it affects crystal's light response uniformity. It was also found that the slow component is highly correlated with the radiation-induced readout noise and may be eliminated spectroscopically by using an optical filter. The slow component is believed to be related to impurities and/or defects in the crystal.**

***Index Terms*— Radiation-induced readout noise (RIN), slow scintillation component, undoped caesium iodide.**

I. Introduction

BECAUSE of its fast scintillation and low cost, undoped CsI crystal has been used to construct crystal calorimeters for the KTeV [1] and super Belle [2]–[4] experiments and has recently been chosen by the Mu2e experiment at Fermilab [5]–[8]. Historically, optical and scintillation properties of undoped CsI crystals have been intensively studied [9]–[20]. There are, however, still two crucial issues to be understood: the slow scintillation component with microseconds decay time (slow component) and the radiation-induced readout noise (RIN).

Undoped CsI crystal samples grown by AMCRYS Inc. (Kharkov), Optomaterials Inc., and Shanghai Institute of Ceramics (SIC) were characterized at the Caltech HEP Crystal Laboratory. The slow component, its effect on crystal's performance, and the RIN were investigated. While our early report was given in the NSS 2016 Conference [21], the detailed results of this paper are presented in this paper. Following this investigation, 72 preproduction undoped CsI crystals were procured from commercial produces and were characterized at the Caltech HEP Crystal Laboratory and the Laboratori Nazionali di Frascati dell' INFN. The results are compared to the Mu2e specifications defined according to physics requirements and presented in the SCINT 2017 Conference [22]. Seven undoped CsI crystal samples of various dimensions from three vendors were investigated. While three samples from Kharkov are of $29 \times 29 \times 230$ mm^3, one from Optomaterials is $30 \times 30 \times 200$ mm^3, and three from SIC are $30 \times 30 \times 200$ mm^3 and $34 \times 34 \times 200$ mm^3. Fig. 1 shows the photograph of the samples tested. All samples are optically polished by manufactures.

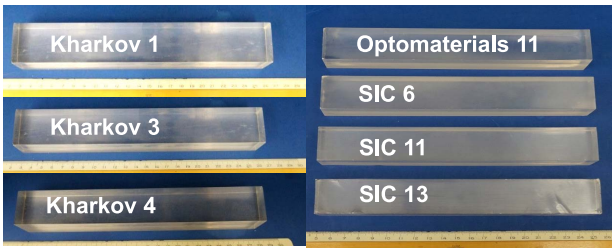

Fig. 1. Undoped CsI samples from Kharkov, Optomaterials, and SIC.

II. Slow Component in Undoped Caesium Iodide Crystals

Crystal's light output (LO), full-width at half-maximum energy resolution (ER) and light response uniformity (LRU) were measured with 200-ns integration time by a Hamamatsu R2059 photomultiplier (PMT) with a bialkali photocathode and a quartz window. We used a LeCroy 2415 HV power supplier which offers an output ripple (rms) of less than 50 mV and a temperature coefficient of ±50 ppm/°C. Since the room temperature of our lab is maintained at 20 °C with an rms instability of 0.2 °C measured over 24 h, the HV instability, thus, is less than 25 ppm for the HAMAMATSU R2059 PMT at 2100 V. The corresponding gain stability of R2059 is less than 250 ppm, or 0.03%. The photocurrent from the PMT was integrated by a LeCroy 3001 charge, voltage, and time in the Q mode. The integration gates were provided by a LeCroy 2323A programmable gate generator. To avoid scratching crystal's soft surfaces, an air gap was used to couple one end of the sample to the PMT while all other five faces of the sample were wrapped with two layers of Tyvek paper.

Manuscript received July 17, 2018; accepted August 30, 2018. Date of publication September 6, 2018; date of current version October 17, 2018. This work was supported in part by the U.S. Department of Energy through the Office of High Energy Physics Program under Award DE-SC0011925, in part by the Fundamental Research Funds for the Central Universities of China, and in part by the Natural Science Funds of China under Grant 11775120.

F. Yang was with HEP, California Institute of Technology, Pasadena, CA 91125 USA. He is now with the Key Laboratory of Weak-Light Nonlinear Photonics, Ministry of Education, School of Physics, Nankai University, Tianjin 300071, China (e-mail: fan@nankai.edu.cn).

L. Zhang, C. Hu, and R.-Y. Zhu are with HEP, California Institute of Technology, Pasadena, CA 91125 USA (e-mail: zhu@hep.caltech.edu).

Color versions of one or more of the figures in this paper are available online at http://ieeexplore.ieee.org.

Digital Object Identifier 10.1109/TNS.2018.2868678

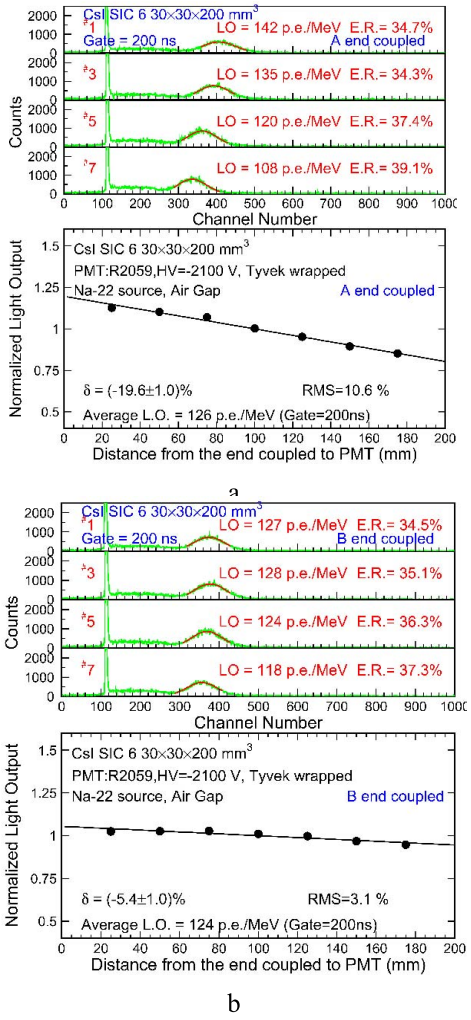

Fig. 2. PHS (top) and LRU (bottom) with (a) A end coupling and (b) B end coupling for sample SIC 6.

Pulse height spectra (PHS) were obtained by aiming a collimated Na-22 source at seven points evenly distributed along the crystal's axis. Na-22 γ -ray peak positions were determined by a simple Gaussian fit. The overall systematic uncertainty in repeated LO measurements is about 1%. Crystal's LO and ER are defined as the average of seven points. Crystal's LRU is defined as the rms value of the seven points. Crystal's LO at seven points were also fit to a linear function

$$\frac{y}{y_{\text{mid}}} = 1 + \delta\left(\frac{x}{x_{\text{mid}}} - 1\right) \tag{1}$$

where y_{mid} represents the LO at the middle point of the crystal, δ provides another representation of the LRU, and x is the distance to the PMT.

Because of its rectangular shape, one of the two ends marked as A and B randomly may be coupled to the PMT. Fig. 2(a) and (b) shows the PHS at points 1, 3, 5, and 7 (top) and the LO as a function of distance to the PMT (bottom) measured for the A and B end coupled to the PMT, respectively, for SIC 6. The LO and ER values are listed in the top plots, and the average LO, rms, and δ values are listed in the bottom plots. Both the rms and δ values are smaller with the B end

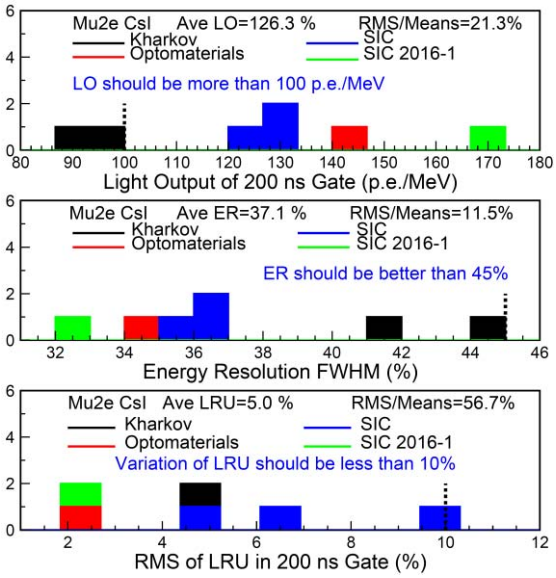

Fig. 3. Summary of LO (top), ER (middle), and LRU (bottom) measured for undoped CsI samples from three vendors.

coupling for SIC 6. CsI is an intrinsic scintillator. Its LRU is affected by both the light production and light propagation in the crystal bulk. While the former may be position dependent due to the density of defects and inclusions introduced during the growth process, the latter is affected, in addition, by crystal's surface quality. To minimize the degradation of calorimeter ER caused by light response nonuniformity, B end may be chosen as the coupling end for this crystal [23].

Fig. 3 summarizes the LO (top), ER (middle), and rms (bottom) values together with the Mu2e specifications (dashed lines). Since the performance of the samples is the coupling end dependent, the average of both coupling ends is used in this figure. The LO of almost all the samples satisfies the specification except two Kharkov samples, presumably because of its slim dimension which increases the light bouncing numbers in the crystal bulk. The sample SIC 2016-1 has the highest LO, which is presumably due to its larger coupling face than the others. The ER of all the samples satisfies the specification, where two Kharkov samples show the worst ER because of their low LO. One SIC sample shows bad LRU, indicating the necessity to improve the crystal surface processing. In a conclusion, commercially available undoped CsI crystals may be used to construct the Mu2e calorimeter.

Fig. 4 shows the LO as a function of integration time measured for three undoped CsI samples from different vendors. In these measurements, a collimated Na-22 source was aimed at 29 and 25 mm from the PMT for 230- and 200-mm-long samples, respectively, which corresponds to the first data point closest to the PMT in Fig. 2. The LO is fit to two exponential decay times. In addition to a fast component with 30-ns decay time, a slow component with a decay time of a few microseconds was observed in Kharkov and Optomaterials samples. No slow component was observed in sample SIC 6, indicating that it is not intrinsic, rather impurities and/or defects related, so can be eliminated through purifying raw material and optimizing crystal growth technique. This conclusion is

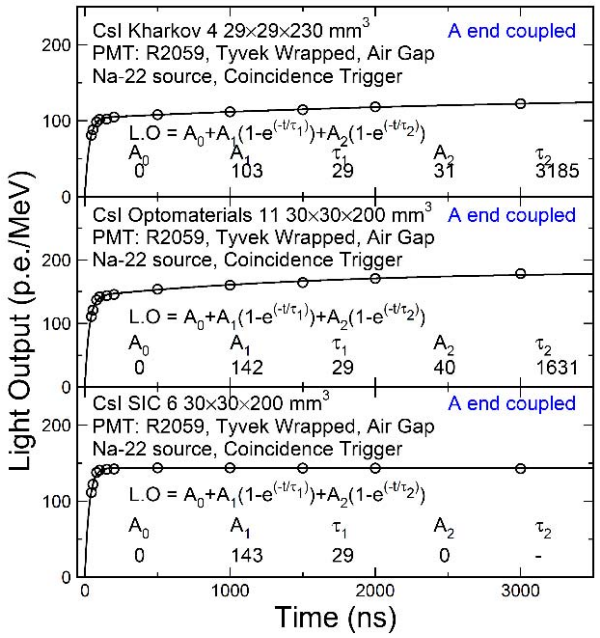

Fig. 4. LO as a function of integration time for CsI samples.

consistent with early suggestions that the slow component is due to Na^+ or CO_3 contamination [19], [24], [25] or intrinsic and extrinsic structure defects [19], [26].

Fig. 5(a)–(c) shows the LO with 200-ns (top) and 3000-ns (middle) integration time and the fast/total ratio (F/T), defined as LO (200 ns)/LO (3000 ns), as a function of the distance to the PMT for Kharkov 4, Optomaterials 11, and SIC 6, respectively. The F/T ratio values are 75%, 84%, and 98% for Kharkov 4, Optomaterials 11, and SIC 6, respectively, indicating that the slow component is sample and vendor dependent. The F/T ratio also decreases from the one end to other in Kharkov 4, which is not observed in Optomaterials 11 and SIC 6. The variation of the F/T ratio would certainly affect the LRU.

Fig. 6 shows a summary of the F/T ratio for all samples together with the Mu2e specification (dashed lines). Most samples except one Kharkov satisfy the F/T ratio specification.

Fig. 7 shows the comparison of X-ray excited luminescence (XEL) spectra for SIC 6 (red curve) and Kharkov 4 (blue curve), which were measured by a Hitachi F-4500 fluorescence spectrophotometer for samples excited by an Amptek E3-T X-ray tube. The result shows almost no slow component in SIC 6 and a high slow component in Kharkov 4. An additional emission peaked at 450 nm was clearly observed in Kharkov 4, which is consistent with the previous investigations [19], [20]. Fig. 7 also shows an FGUV-11 bandpass filter with the bandwidth of 275–375 nm which was used to select the main emission and cut the slow component in undoped CsI.

Although not applicable in the Mu2e calorimeter, the use of the FGUV-11 bandpass filter is investigated to understand the nature of the slow component in CsI. Fig. 8 shows the comparison of LO as a function of integration time measured with (red square) and without (black circles) the FGUV-11 filter for two CsI samples with slow component: Kharkov 4 and Optomaterials 11. The slow component was completely eliminated by the filter in both samples. As a consequence, however, the LO of these samples was reduced to about half by using this filter.

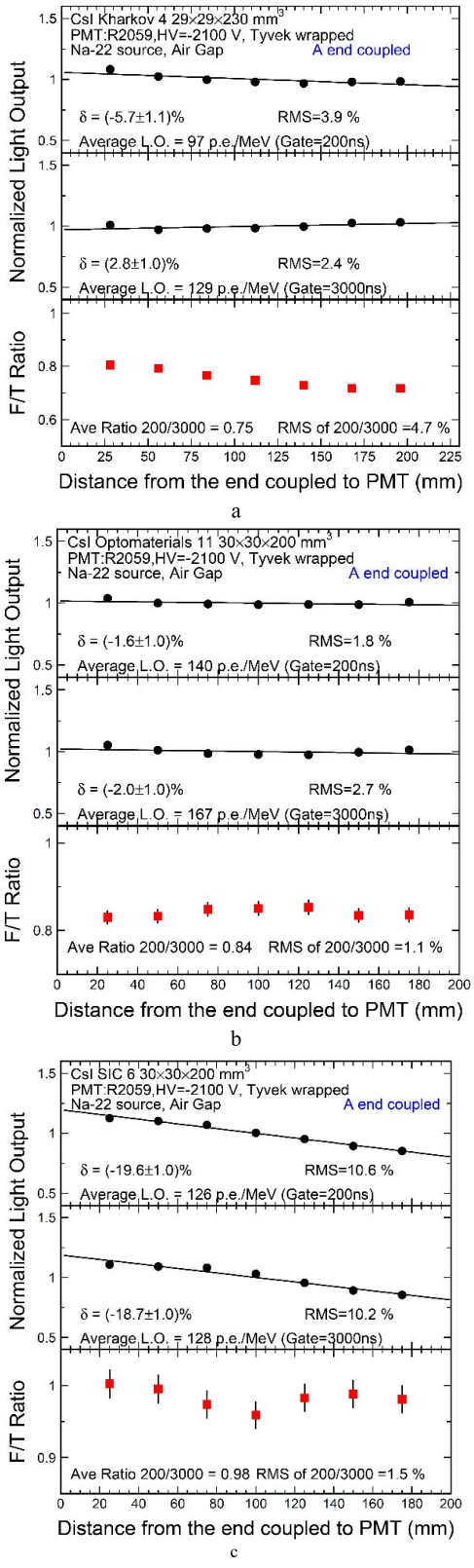

Fig. 5. LO with 200-ns (top) and 3000-ns (middle) integration time and the F/T ratios (bottom) measured at seven points along the CsI samples from three vendors. (a) Kharkov 4. (b) Optomaterials 11. (c) SIC 6.

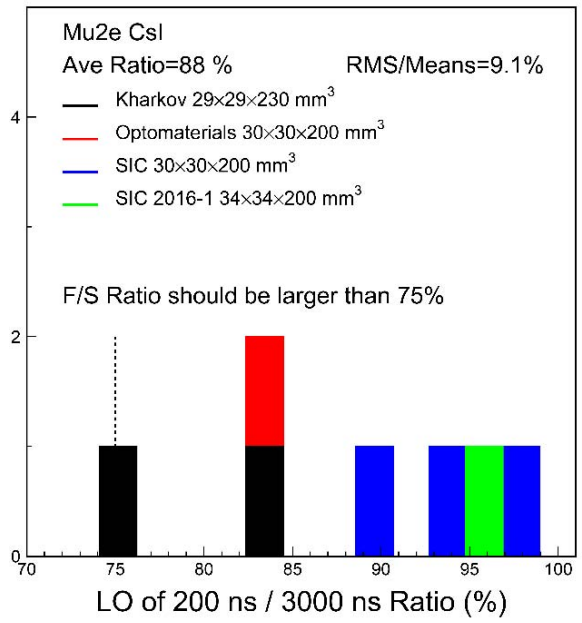

Fig. 6. Summary of the F/T ratio.

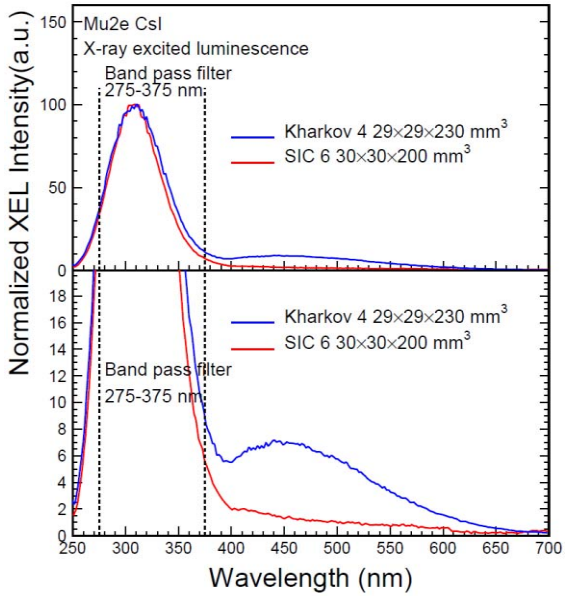

Fig. 7. XEL spectra (top) and their expanded view (bottom) for undoped CsI samples with different levels of slow component.

Fig. 9(a) and (b) shows the LO with 200-ns (top) and 3000-ns (middle) integration time and the F/T ratio (bottom) as a function of the distance to the PMT measured with the FGUV-11 bandpass filter for Kharkov 4 and Optomaterials 11, respectively. Both the F/T ratio and the LRU are improved with the FGUV-11 bandpass filter, confirming that eliminating the slow component improves the LRU for undoped CsI crystals.

Radiation hardness of undoped CsI samples was measured with integrated doses of 1, 10, and 100 krad. All samples were irradiated following the same procedure. The crystals were irradiated to 1 krad at 30 rad/h, and then to 10 and 100 krad at 7 krad/h. The total irradiation process took about two days. Since no damage recovery was observed in CsI crystals at room temperature, there is no dose rate

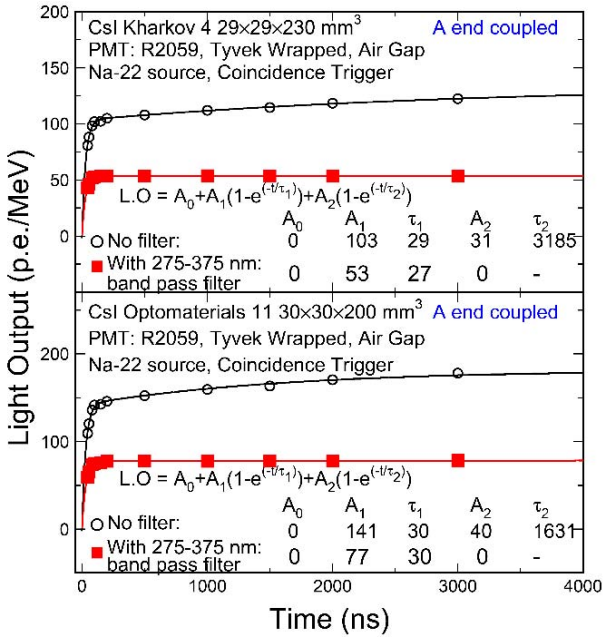

Fig. 8. LO as a function of integration time measured with (red squares) and without (black circles) the FGUV-11 bandpass filter.

dependence [27]. Fig. 10 shows the normalized LO with 200-ns (top) and 3000-ns (middle) integration time and the F/T ratio (bottom) as a function of the integrated dose for four undoped CsI samples. The samples Kharkov 4 and SIC 2016-1 show a good radiation hardness with an LO loss of about 20% and 25% for 200- and 3000-ns integration time, respectively, after 100 krad. The samples Optomaterials 11 and SIC 11, however, show a poor radiation hardness, whose LO loss is about 55% and 60% for 200- and 3000-ns integration time, respectively, after 100 krad. Since Kharkov 4 and SIC 2016-1 have very different F/T ratios of 75% and 95%, this observation indicates that the slow component does not affect the radiation hardness of undoped CsI crystals. Rather, it is known that radiation hardness in halide crystals is related to oxygen contamination [27]. On the other hand, it is also interesting to note that the F/T ratio increases with increased integrated dose.

III. Radiation-Induced Photocurrent and RIN

The radiation environment of the Mu2e experiment is 10-krad ionization dose and 2×10^{11} n/cm^2 each year expected at the hottest region with a factor of three safety margins. Assuming 230 days run (2×10^7 s) per year, the expected radiation environment at the hottest region is 1.8 rad/h for ionization dose and 1×10^4 n/cm^2/s for neutron fluence [22]. Phosphorescence induced by such radiation environment in undoped CsI crystals produces RIN. The energy equivalent RIN (σ) is defined as the standard deviation of the photoelectron number (Q) in the readout gate

$$\frac{\sqrt{Q}}{\mathrm{LO}}\ \mathrm{MeV}. \tag{2}$$

We define F as the radiation-induced photoelectron numbers per second, which can be extracted by the photocurrent in the

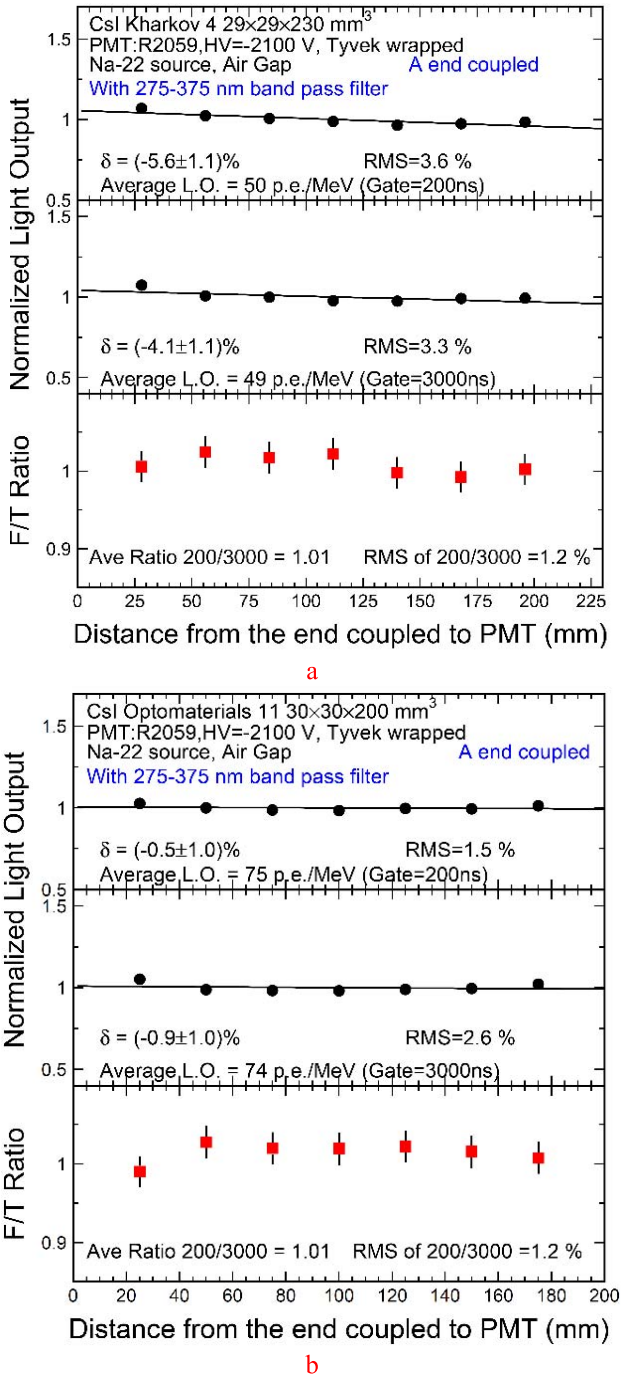

Fig. 9. LO measured with 200-ns (top) and 3000-ns (middle) integration time and the F/T ratios (bottom) measured with the FGUV-11 bandpass filter at seven points for (a) Kharkov 4 and (b) Optomaterials 11.

PMT

$$F = \frac{\text{Photocurrent}}{\text{Charge}_{\text{electron}} \times \text{Gain}_{\text{PMT}}} \Big/ \text{Dose rate}_{\gamma-\text{ray}}(\text{or Flux}_{\text{neutron}}). \quad (3)$$

Fig. 11 shows the setup used for the measurement of γ-ray-induced photocurrent. A Co-60 source was used to excite the crystal. The γ-ray-induced photocurrent was measured by the same Hamamatsu PMT R2059 used to measure the LO. The setup for neutron-induced photocurrent measurement

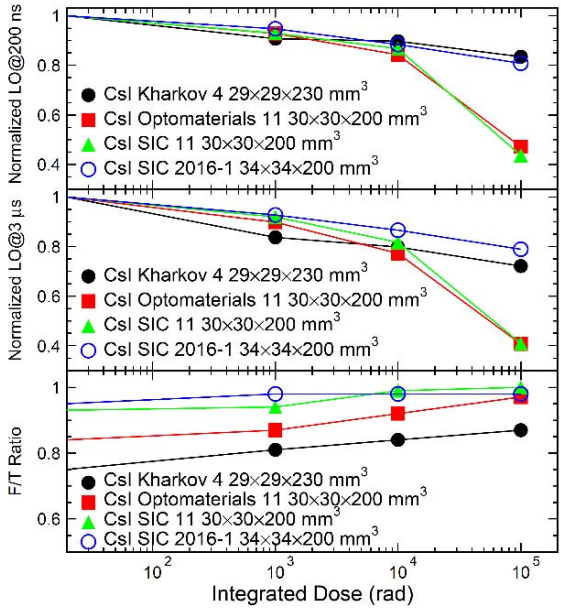

Fig. 10. Normalized LO with 200-ns (top) and 3000-ns (middle) integration time and the F/T ratio (bottom) are shown as a function of the integrated dose for undoped CsI samples.

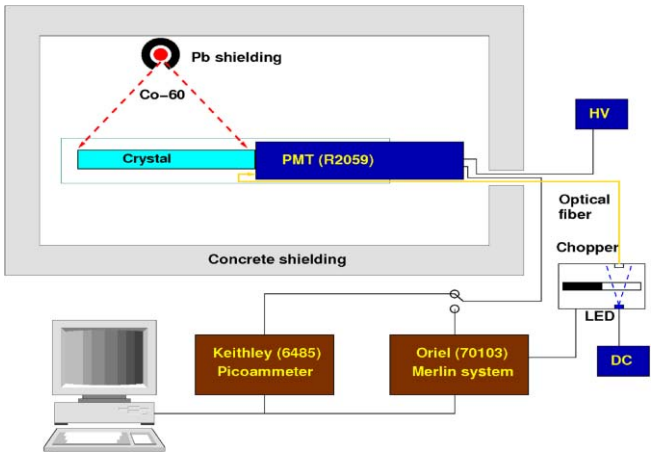

Fig. 11. Setup of γ-ray-induced photocurrent measurement.

is similar, except that the Co-60 source was replaced by Cf-252 sources.

Fig. 12 shows the history of the photocurrent before (dark current), during (radiation-induced photocurrent), and after (afterglow) γ-ray irradiations for three undoped CsI samples with slow component: Kharkov 4, Optomaterials 11, and SIC 11, under a dose rate of 1.8 rad/h. In these measurements, the samples were wrapped with Tyvek paper and coupled to the PMT with an air gap. They were placed in a dark room until the dark current reached an equilibrium, and then the source was applied and removed. The afterglow in all three samples can be fit to three time constants of 0.8, 4.7, and 22.8 h, indicating that the same nature of afterglow in these samples.

Fig. 13 shows a similar history of photocurrent for sample SIC 6 with a very small slow component. Its afterglow can be fit to two time constants of 0.4 and 3 h, indicating that the decay constant of 22.8 h in the samples with slow component

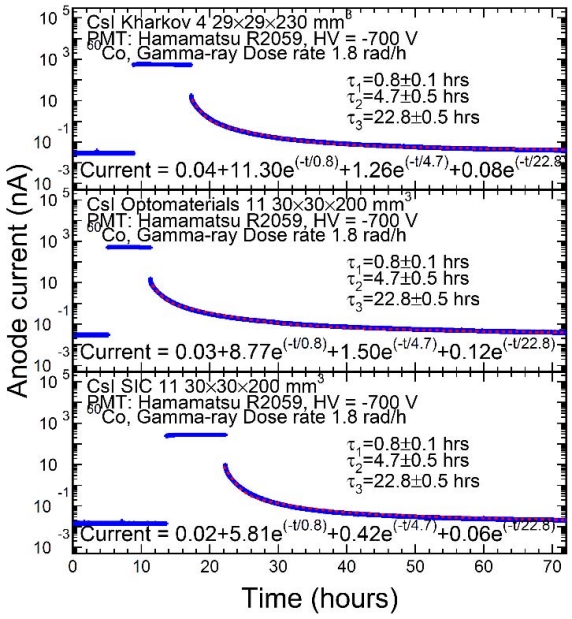

Fig. 12. History of photocurrent measured before, during, and after γ-ray irradiation for undoped CsI samples with the slow component.

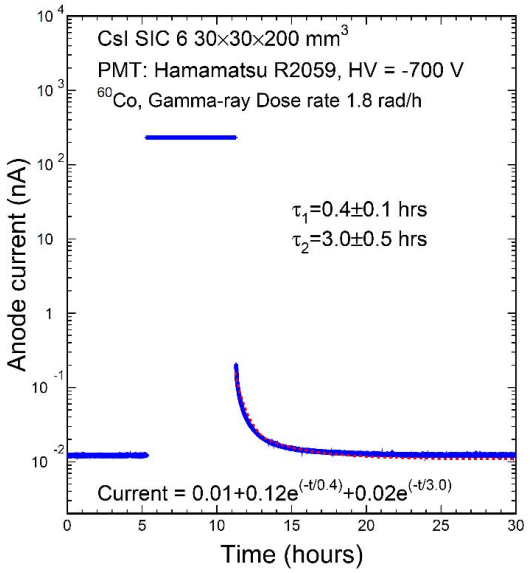

Fig. 13. History of photocurrent measured before, during, and after γ-ray irradiation for undoped CsI samples without slow component.

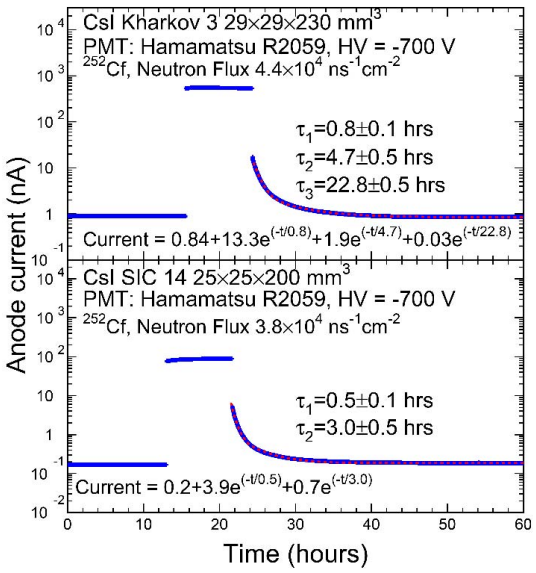

Fig. 14. History of photocurrent measured before, during, and after neutron irradiation for two undoped CsI crystals.

TABLE I

VOLUME NORMALIZED γ-RAY-INDUCED READOUT NOISE

Sample	Dimensions (cm^3)	LO of 200 ns gate (p.e./MeV)	Dark Current (nA)*	Photo current (nA)*	F (p.e./s/rad/hr)*	σ (MeV)*
Kharkov4	2.9×2.9×23	96	0.035	679	6.68E+09	5.11E-01
Opto 11	3×3×20	140	0.039	663	6.53E+09	3.46E-01
SIC 6	3×3×20	125	0.015	296	2.91E+09	2.59E-01
SIC 11	3×3×20	128	0.018	330	3.25E+09	2.67E-01
SIC 13	3×3×20	130	0.026	461	4.54E+09	3.11E-01

TABLE II

VOLUME NORMALIZED NEUTRON-INDUCED READOUT NOISE

Sample	Dimensions (cm^3)	LO of 200 ns gate (p.e./MeV)	Dark Current (nA)*	Photo current (nA)*	F ($p.e./n/cm^2$)*	σ (MeV)*
Kharkov 3	2.9×2.9×23	88	0.08	112	5.01E+04	1.1E-01
SIC 2014	2.5×2.5×20	140	0.013	165	8.68E+04	9.4E-02

* Dark current, photocurrent, F and σ are corrected to the volume 3.4×3.4×20 cm^3.

(Kharkov 4, Optomaterials 11, and SIC 11) is directly related to the slow component.

Fig. 14 shows a history of photocurrent for Kharkov 3 with slow component and SIC 14 without slow component, which was measured before, during, and after fast neutron irradiation at 1×10^4 n/cm^2/s. Once again, the afterglow requires three/two time constants for undoped CsI crystals with/without slow component. We also notice that the time constants for the neutron-induced afterglow are consistent with that induced by γ-rays, indicating that it may be caused by the γ-ray background from the Cf-252 sources.

Tables I and II summarize the dark current, photocurrent, F, and the RIN (σ) induced by γ-rays and neutrons, respectively. All the numbers were corrected to the crystal volume of $3.4 \times 3.4 \times 20$ cm^3 for the Mu2e experiment. It is also clear that the RIN induced by γ-rays is larger than that from fast neutrons from the Cf-252 sources even without subtracting the γ-ray background.

Fig. 15 shows the RIN values induced by γ-rays in undoped CsI crystals from three vendors. Fig. 15 also shows the Mu2e specification (dashed lines) of 0.6 MeV. While all samples satisfy the specification, it is clear that the SIC samples have relatively lower RIN values than the samples from Kharkov and Optomaterials.

Fig. 16 shows two correlations between the dark current (top) and the RIN induced by γ-rays (bottom) versus the F/T ratio, where the crystal volume was normalized to $3.4 \times 3.4 \times 20$ cm^3. Fig. 16 also shows the linear correlation

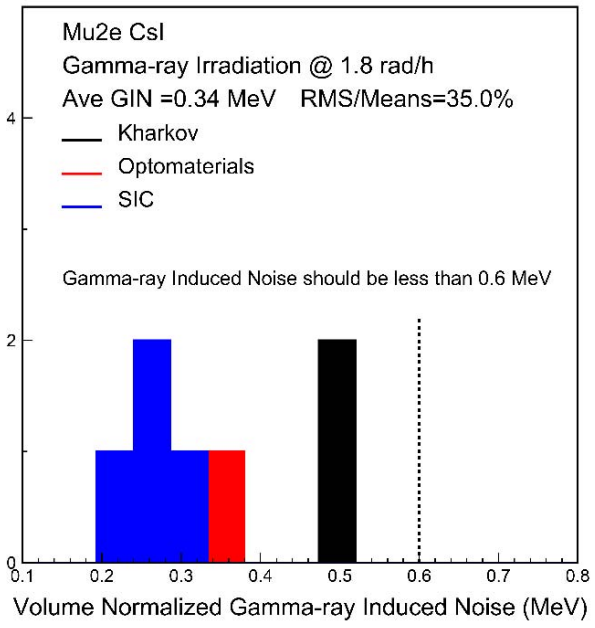

Fig. 15. RIN induced by γ-rays for undoped CsI crystals from three vendors.

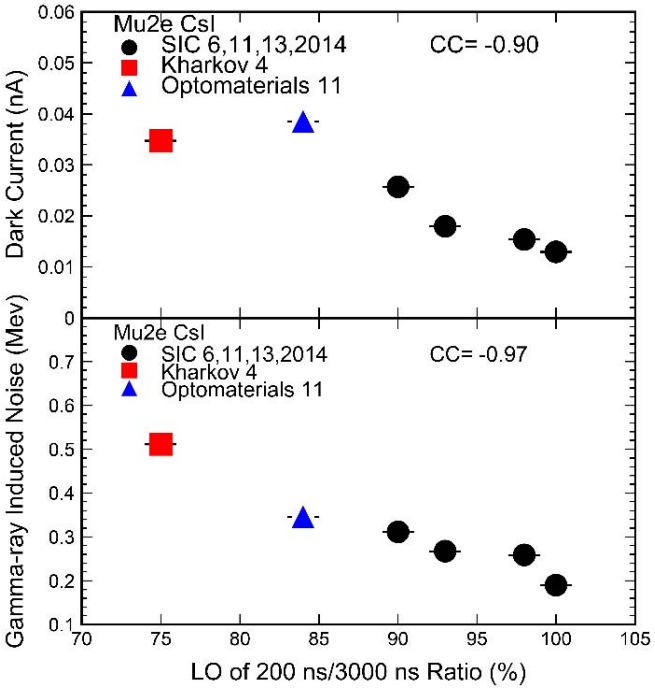

Fig. 16. Correlations between the dark current (top) and the RIN induced by γ-rays (bottom) versus the F/T ratio.

coefficients (CC), defined as

$$\mathrm{CC} = \frac{\sum(x-\bar{x})(y-\bar{y})}{\sqrt{\sum(x-\bar{x})^2 \sum(y-\bar{y})^2}}. \tag{4}$$

Excellent correlations at a level of 90% and 97% are observed between the dark current and the RIN induced by γ-rays, respectively, versus the F/T ratio, indicating that the suppression of the slow component in undoped CsI crystals is important for crystal quality control for the Mu2e experiment. Similarly, Fig. 17 shows an additional correlation observed between the dark current and the RIN induced by γ-rays.

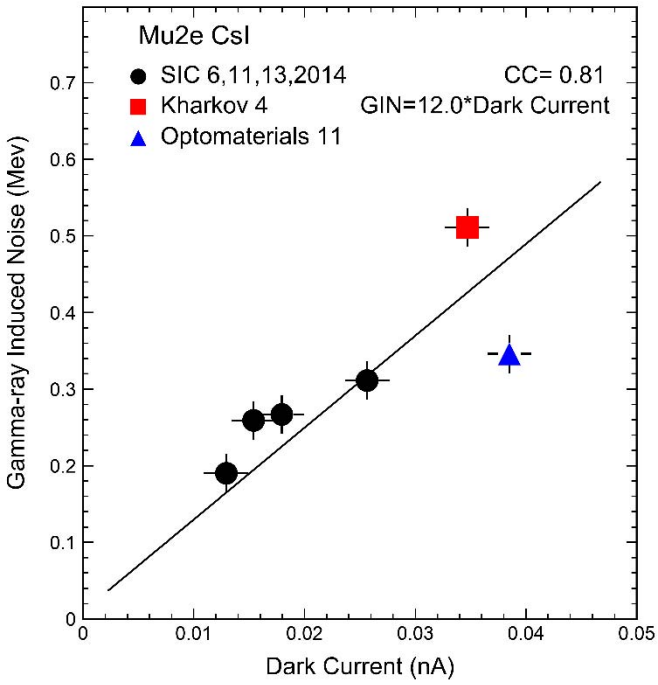

Fig. 17. Correlation between the dark current and the γ-ray-induced noise.

These excellent correlations have also been confirmed by the recent results obtained with 72 preproduction undoped CsI crystals measured by the Mu2e experiment [22]. These good correlations indicate that the RIN induced by γ-rays may be estimated by measuring the F/T ratio or the dark current, offering more convenient approaches to characterize undoped CsI crystals.

IV. Conclusion

Undoped CsI crystals are chosen for the Mu2e experiment at Fermilab. Its fast emission peaked at 310 nm with 30-ns decay time requires photodetector with the UV extended response. Large size undoped CsI crystal samples produced by Kharkov, Optomaterials, and SIC were investigated at Caltech. Most samples from three vendors satisfy the Mu2e specifications, indicating that the growth technique of undoped CsI crystals is mature in the commercial market.

A slow component peaked at 450 nm with microseconds decay time is observed in undoped CsI crystals. We believe that it is impurities or defects related. Since, the distribution of the slow component is not uniform along the crystal, the LRU of the crystal would be affacted, so is the ER of the calorimeter. The slow component in undoped CsI may be completely eliminated spectroscopically by inserting an optical filter with a price for a reduced fast LO.

The photocurrent induced by γ-rays and neutrons was measured for undoped CsI crystals and were used to extract RIN. Excellent correlations are observed between the dark current, the RIN induced by γ-rays, and F/T ratio, indicating the importance to eliminate the slow component for undoped CsI crystals. These correlations also offer a convenient crystal quality control approach by measure the F/T ratio and/or the dark current for undoped CsI crystals.

ACKNOWLEDGMENT

The authors would like to thank the Mu2e collaboration for providing the undoped CsI samples discussed in this paper as well as many useful discussions.

REFERENCES

[1] V. Prasad, "Performance of the cesium iodide calorimeter at the KTeV experiment at Fermilab," *Nucl. Instrum. Methods Phys. Res. A, Accel. Spectrom. Detect. Assoc. Equip.*, vol. 461, nos. 1–3, pp. 341–343, 2001.

[2] A. Aloisio *et al.*, "A pure CsI calorimeter for the Belle II experiment at SuperKEKB," *Nucl. Instrum. Methods Phys. Res. A, Accel. Spectrom. Detect. Assoc. Equip.*, vol. 824, pp. 704–709, Jul. 2016.

[3] A. Kuzmin and For the Belle ECL team, "Endcap calorimeter for SuperBelle based on pure CsI crystals," *Nucl. Instrum. Methods Phys. Res. A, Accel. Spectrom. Detect. Assoc. Equip.*, vol. 623, no. 1, pp. 252–254, 2010.

[4] A. Boyarintsev *et al.*, "Study of radiation hardness of pure CsI crystals for Belle-II calorimeter," *J. Instrum.*, vol. 11, p. 03013, Mar. 2016.

[5] N. Atanov *et al.*, "The Mu2e crystal calorimeter," *J. Instrum.*, vol. 12, no. 9, p. P09017, 2017.

[6] N. Atanov *et al.*, "The calorimeter of the Mu2e experiment at Fermilab," *J. Instrum.*, vol. 12, no. 1, p. C01061, 2017.

[7] N. Atanov *et al.*, "Design and status of the Mu2e electromagnetic calorimeter," *Nucl. Instrum. Methods Phys. Res. A, Accel. Spectrom. Detect. Assoc. Equip.*, vol. 824, pp. 695–698, Jul. 2016.

[8] F. Yang, L. Zhang, and R.-Y. Zhu, "Gamma-ray induced radiation damage up to 340 Mrad in various scintillation crystals," *IEEE Trans. Nucl. Sci.*, vol. 63, no. 2, pp. 612–619, Apr. 2016.

[9] Z.-Y. Wei and R.-Y. Zhu, "A study on undoped CsI crystals," *Nucl. Instrum. Methods Phys. Res. A, Accel. Spectrom. Detect. Assoc. Equip.*, vol. 326, no. 3, pp. 508–512, 1993.

[10] I. V. Bedny *et al.*, "Study of the radiation hardness of the undoped CsI crystals," *Nucl. Instrum. Methods Phys. Res. A, Accel. Spectrom. Detect. Assoc. Equip.*, vol. 598, pp. 273–274, Jan. 2009.

[11] M. Angelucci *et al.*, "Longitudinal uniformity, time performances and irradiation test of pure CsI crystals," *Nucl. Instrum. Methods Phys. Res. A, Accel. Spectrom. Detect. Assoc. Equip.*, vol. 824, pp. 678–680, Jul. 2016.

[12] S. Keszthelyi-Lándori, I. Földvári, R. Voszka, Z. Fodor, and Z. Seres, "Decay time measurements on 'pure' CsI scintillators prepared by different methods," *Nucl. Instrum. Methods Phys. Res. A, Accel. Spectrom. Detect. Assoc. Equip.*, vol. 303, no. 2, pp. 374–380, 1991.

[13] E. Frlez *et al.*, "Light response of pure CsI calorimeter crystals painted with wavelength-shifting lacquer," *Nucl. Instrum. Methods Phys. Res. A, Accel. Spectrom. Detect. Assoc. Equip.*, vol. 459, no. 3, pp. 426–439, 2001.

[14] C. Amsler *et al.*, "Temperature dependence of pure CsI: Scintillation light yield and decay time," *Nucl. Instrum. Methods Phys. Res. A, Accel. Spectrom. Detect. Assoc. Equip.*, vol. 480, nos. 2–3, pp. 494–500, 2002.

[15] A. Ejiri and S. Kubota, "VUV photoelectron dynamics in undoped cesium halide and impurity (Tl and Na) doped CsI; absolute photoemission total yield, Auger free luminescence, and STE luminescence," *Surf Rev Lett*, vol. 9, pp. 447–454, 2002.

[16] M. Moszynski *et al.*, "Energy resolution and non-proportionality of the light yield of pure CsI at liquid nitrogen temperatures," *Nucl. Instrum. Methods Phys. Res. A, Accel. Spectrom. Detect. Assoc. Equip.*, vol. 537, nos. 1–2, pp. 357–362, 2005.

[17] Z. Wu, B. Yang, and P. D. Townsend, "Radioluminescence and thermoluminescence properties of X-ray-irradiated pure CsI," *J Lumin*, vol. 128, no. 7, pp. 1191–1196, 2008.

[18] J. Liu, M. Yamashita, and A. K. Soma, "Light yield of an undoped CsI crystal coupled directly to a photomultiplier tube at 77 Kelvin," *J. Instrum.*, vol. 11, no. 10, p. P10003, 2016.

[19] M. Moszynski *et al.*, "Energy resolution and slow components in undoped CsI crystals," *IEEE Trans. Nucl. Sci.*, vol. 63, no. 2, pp. 459–466, Apr. 2016.

[20] G.-H. Ren *et al.*, "Luminescence and decay time properties of pure CsI crystals," *J. Inorganic Mater.*, vol. 32, no. 2, pp. 169–174, 2017.

[21] F. Yang, L. Zhang, and R.-Y. Zhu, "Slow component and radiation induced readout noise in undoped CsI crystals," in *Proc. IEEE Nucl. Sci. Symp., Med. Imag. Conf. Room-Temp. Semiconductor Detector Workshop (NSS/MIC/RTSD)*, Oct. 2016, pp. 1–4.

[22] N. Atanov *et al.*, "Quality assurance on undoped CsI crystals for the Mu2e experiment," *IEEE Trans. Nucl. Sci.*, vol. 65, no. 2, pp. 752–757, Feb. 2018.

[23] D. J. Graham and C. Seez, "Simulation of longitudinal light collection uniformity in PbWO4 crystals," Eur. Lab. Part. Phys., Geneva, Switzerland, Tech. Rep. CMS-NOTE-1996-0021996, Oct. 1996.

[24] V. I. Goriletsky, B. V. Grinyov, A. M. Panova, K. V. Shakhova, E. L. Vinograd, and S. P. Korsunov, "Kinetic and scintillation characteristics of CsI(Na) crystals grown under melt mixing," *Nucl. Instrum. Methods Phys. Res. B, Beam Interact. Mater. At.*, vol. 159, nos. 1–2, pp. 111–115, 1999.

[25] E. L. Vinograd, V. I. Goriletsky, and A. N. Panova, "Optical and scintillation characteristics of CsI crystals with impurity Cs_2CO_3," *Opt. Spectrosc.*, vol. 69, p. 1185, Jan. 1990.

[26] P. R. Beck, S. A. Payne, S. Hunter, L. Ahle, N. J. Cherepy, and E. L. Swanberg, "Nonproportionality of scintillator detectors. V. Comparing the gamma and electron response," *IEEE Trans. Nucl. Sci.*, vol. 62, no. 3, pp. 1429–1436, Jun. 2015.

[27] R.-Y. Zhu, "Radiation damage in scintillating crystals," *Nucl. Instrum. Methods Phys. Res. A, Accel. Spectrom. Detect. Assoc. Equip.*, vol. 13, nos. 2–3, pp. 297–311, 1998.